https://doi.org/10.5194/egusphere-2026-6618
Preprint. Discussion started: 16 November 2026
© Author(s) 2026. CC BY 4.0 License.

Identifying surface-level O_3 photochemical regimes using meteorology-adjusted satellite observations and statistical and machine learning models in South Korea

Chaoreum Kang[1], Hyung Joo Lee[1]

[1]Division of Environmental Science and Engineering, Pohang University of Science and Technology (POSTECH), Pohang, Gyeongbuk 37673, Republic of Korea

Correspondence to: Hyung Joo Lee (hyungjoolee@postech.ac.kr)

Abstract. Ground-level ozone (O_3) is a persistent urban and regional air quality challenge because its production responds nonlinearly to nitrogen oxides (NO_x) and volatile organic compounds (VOCs) and is strongly influenced by meteorological conditions. The satellite-based ratio of formaldehyde (HCHO) to nitrogen dioxide (NO_2) (i.e., HCHO/NO_2) is a reliable indicator of O_3 photochemical regimes that distinguishes whether O_3 production is NO_x-limited or NO_x-saturated; however, the corresponding regime thresholds remain poorly constrained. A new framework was developed to identify refined regime thresholds by integrating ground and satellite observations, while accounting for meteorological variability using statistical and machine learning models. When applied to O_3 air pollution in South Korea from 2019 to 2023, the framework revealed robust O_3 photochemical regimes based on province-specific regime thresholds with 34% lower uncertainty than conventional approaches. In addition, the regime thresholds reasonably captured regional characteristics of O_3 responses to NO_2 perturbations, with the scenario-specific correlations of 0.57–0.75. A meta-analysis indicated that a unified nationwide regime threshold was not feasible and that applying the regional regime thresholds of 1.8–3.9 provided a more reasonable basis for O_3 photochemical regime inferences. The framework provides transferable, meteorology-adjusted guidance for designing region-specific NO_x and VOC control strategies, supporting more effective O_3 air quality management.

1 Introduction

Surface-level ozone (O_3) is a secondary air pollutant formed by atmospheric photochemical reactions. The photochemical reactions are initiated by the oxidation of volatile organic compounds (VOCs), releasing organic free radicals, which then react with nitrogen oxides (NO_x = NO + NO_2) and produce O_3 (Seinfeld and Pandis, 2016). Due to the intrinsic complexity of the net O_3 production ($P(O_3)$), defined as the O_3 formation rate minus the loss rate, it shows non-linear responses to the precursor gases, NO_x and VOCs. In NO_x-limited environments (NO_x << VOCs), the $P(O_3)$ is proportional to NO_x levels. However, in NO_x-saturated environments (NO_x >> VOCs), the $P(O_3)$ tends to be inversely proportional to NO_x levels and responds more sensitively to VOC than to NO_x. The concept of $P(O_3)$ sensitivity identifies the controlling precursor gas for

https://doi.org/10.5194/egusphere-2026-6618
Preprint. Discussion started: 16 November 2026
© Author(s) 2026. CC BY 4.0 License.

$P(O_3)$ and thus serves as a critical basis for establishing emission control strategies to effectively mitigate surface-level O_3 air pollution.

The ratio of formaldehyde (HCHO) to nitrogen dioxide (NO_2) (i.e., $HCHO/NO_2$) has been used as a reasonable indicator for $P(O_3)$ sensitivity (Souri et al., 2023; Souri et al., 2020; Martin et al., 2004; Johnson et al., 2023; Acdan et al., 2023; Duncan et al., 2010; Schroeder et al., 2017). HCHO is a ubiquitous by-product of VOC oxidation, reflecting recent VOC reactivity associated with the radical pool (Wolfe et al., 2016). Similarly, NO_2 serves as a proxy for NO_x, representing ambient NO_x abundance. When the $HCHO/NO_2$ ratio exceeds the regime threshold, the environment is classified as NO_x-limited; otherwise, it is classified as NO_x-saturated. The regime threshold theoretically marks the $P(O_3)$ sensitivity transition (i.e., the transitional regime) where the proportion of precursor gases becomes the most favorable for $P(O_3)$. The $HCHO/NO_2$ is directly observable, offering a clear advantage over other indicators that require extensive *in situ* measurements of trace gases and radical species, as well as substantial computational resources for running atmospheric chemistry models such as chemical transport models (CTMs) or box models (Kleinman, 2005; Kleinman et al., 1997; Kleinman et al., 2001; Sillman, 1999; Sillman and He, 2002). Moreover, satellite-based observations provide continuous global monitoring of $HCHO/NO_2$, allowing comprehensive assessment of O_3 photochemical regimes across broad spatiotemporal scales.

A key challenge in O_3 photochemical regime assessment based on $HCHO/NO_2$ has been the accurate estimation of spatially variant regime thresholds for HCHO/NOss$_2$. Atmospheric chemistry models constrained by diverse *in situ* measurements have attempted to estimate them (Schroeder et al., 2017; Souri et al., 2020; Souri et al., 2023). Such observationally constrained modeling was generally confined to specific field campaigns and thus had insufficient spatiotemporal coverage to derive a representative estimate of the regime threshold or to support up-scaling to broader spatial scales (e.g., province-wide or nation-wide applications) (Whalley et al., 2021; Xiong et al., 2023). Without sufficient observational constraints, inaccuracies in the underlying physics and emission inventories of the models may lead to discrepancies between simulated fields and observations (Wang et al., 2015; Silvern et al., 2019; Schroeder et al., 2017; Keller et al., 2021). To address these limitations, empirical approaches using continuous ground and satellite-based observations have been adopted to derive the regime thresholds (Jin et al., 2020; Li et al., 2024; Ren et al., 2022; Ren et al., 2024; Wang et al., 2021). Despite extensive spatiotemporal coverage and intuitive results based on real-world observations from the target region, empirical approaches did not effectively account for the key drivers of surface-level O_3, which is affected not only by $P(O_3)$ sensitivity but also by meteorological conditions. Therefore, the empirical approaches attributing all O_3 variations to $P(O_3)$ sensitivity without excluding meteorological influences can bias the identification of $P(O_3)$ sensitivity transitions, leading to inaccurate regime thresholds and mischaracterization of the O_3 photochemical regimes. Another critical limitation was the inadequate characterization of uncertainty in the estimated regime thresholds, which has either been overlooked or shown to be considerable in previous studies. This raises concerns about the reliability of regime threshold estimates and consequently limits the practical applicability of the $HCHO/NO_2$ for policymakers designing effective O_3 mitigation strategies.

https://doi.org/10.5194/egusphere-2026-6618
Preprint. Discussion started: 16 November 2026
© Author(s) 2026. CC BY 4.0 License.

To address these research gaps, statistical and machine learning frameworks were developed to infer refined regime thresholds for $HCHO/NO_2$. These multivariate empirical models have rarely been used in O_3 photochemical regime assessments; the models, relying exclusively on measured variables, provided reliable and robust insights into O_3 chemistry accounting for meteorological variations. The framework was applied to O_3 air pollution in South Korea for 2019–2023. Province-level regime thresholds were derived to categorize the nationwide O_3 photochemical regimes while reflecting their spatial heterogeneity. The categorized O_3 photochemical regimes were validated by comparing them with the O_3 responses under multiple NO_x perturbation scenarios. The robust regime thresholds and corresponding photochemical regimes are expected to provide regional characteristics of O_3 chemistry and scientific guidance for future O_3 precursor gas reduction pathways to effectively mitigate O_3 air pollution and its associated health risks.

2 Data and Methodology

2.1 Surface-level O_3 measurements

Hourly surface-level ambient O_3 concentrations were obtained from air quality monitors in South Korea for 2019–2023 (Korea Environment Corporation, 2024). To be paired with daily TROPOspheric Monitoring Instrument (TROPOMI) retrievals, daily O_3 concentrations were calculated by averaging hourly O_3 measurements at 13:00–14:00 local time. Air quality monitors adjacent to the coast, where the paired TROPOMI retrievals can be biased due to the differences in surface albedo (Acdan et al., 2023; Johnson et al., 2023), were excluded from the subsequent analysis. Consequently, 424 monitors (406 urban and 18 suburban monitors) were retained, excluding Jeju Island where all available monitors were located adjacent to the coast.

2.2 Satellite HCHO and NO_2 retrieval

HCHO and NO_2 tropospheric column density products (Level 2) of TROPOMI were obtained over South Korea for 2019–2023 (European Space Agency, 2020, 2021). TROPOMI is a payload of the Copernicus Sentinel 5 Precursor (S5P) satellite, providing daily HCHO and NO_2 levels at approximately 13:30 local sun time with a spatial resolution of 3.5 km × 5.5 km (De Smedt et al., 2022; Van Geffen et al., 2019; De Smedt et al., 2018; Boersma et al., 2018). To assure data quality, TROPOMI HCHO and NO_2 observations with quality assurance values less than 0.5 were excluded from subsequent analysis (Romahn et al., 2022; Eskes et al., 2024). The valid HCHO and NO_2 observations whose pixel centroids fell within a given 5 km × 5 km grid cell were averaged to represent daily HCHO and NO_2 levels of that grid cell, respectively. The daily HCHO and NO_2 levels were then paired with daily surface-level O_3 measurements of the same grid cell.

https://doi.org/10.5194/egusphere-2026-6618
Preprint. Discussion started: 16 November 2026
© Author(s) 2026. CC BY 4.0 License.

2.3 Meteorological data

Hourly meteorological parameters were obtained from ground weather stations and re-analysis data products across South Korea for 2019–2023. We selected meteorological parameters that have been reported to substantially influence surface-level O_3 (Shin and Lee, 2024; Yao et al., 2024; Jin et al., 2017; Kusumaningtyas et al., 2024; Li et al., 2023), and its precursor gases simultaneously (Lee et al., 2023; Wang et al., 2025; Zhang et al., 2024; Li et al., 2021). Surface-level hourly temperature (℃), wind speed (m s^{-1}), and relative humidity (%) were obtained from 220 weather stations operated by the Korea Meteorological Administration (KMA) (Korea Meteorological Administration, 2025). The stations were retained when at least 75% of their observations were valid throughout the study period. Hourly total cloud cover (unitless) and boundary layer height (m) were provided by the 5th generation European Centre for Medium-Range Weather Forecasts (ECMWF) re-analysis (ERA5) with 0.25° × 0.25° resolution (Hersbach, 2023). Hourly surface net solar radiation (J m^{-2}) and surface pressure (Pa) were obtained from the land component of ERA5 (ERA5-Land) with 0.1° × 0.1° resolution (Muñoz Sabater, 2019). All the meteorological parameters from weather stations, ERA5, and ERA5-Land were assigned to the nearest 5 km × 5 km grid cells and were converted into daily basis by averaging data at 13:00–14:00 local time. The mean distance from the grid cell centroids to the weather stations and the centroids of ERA5 and ERA5-Land data was 4.64 km (25th–75th percentile = 2.33–6.04 km), 9.95 km (standard deviation (SD) = 3.60), and 4.06 km (SD = 1.97), respectively.

2.4 Statistical models for identifying regime thresholds

We used a generalized additive model (GAM) to determine the regime thresholds while accounting for meteorological variations. GAM is a generalized linear model with linear predictors involving a sum of smooth functions of covariates (Hastie and Tibshirani, 1986; Hastie, 2017; Wood, 2017; Pedersen et al., 2019). The model facilitates non-linear dependency of a target variable on explanatory variables with smoothing splines, whose degree of smoothness is optimized using generalized cross validation (GCV) on the training data, as implemented in python package '*pyGAM*' (Servén and Brummitt, 2018). Based on its data-driven structure, GAMs capture the non-linear effects of P(O_3) sensitivity and local meteorology on O_3 levels directly from observations (Lee et al., 2023):

$$\begin{aligned} O_{3,ijk} = \beta_{0,i} + s_{1,i}(HCHO_{ijk}/NO_{2,ijk}) + s_{2,i}(TEMP_{ijk}) + s_{3,i}(SSR_{ijk}) \\ +s_{4,i}(RH_{ijk}) + s_{5,i}(BLH_{ijk}) + s_{6,i}(TCC_{ijk}) + s_{7,i}(SP_{ijk}) + s_{8,i}(WS_{ijk}) + \varepsilon_{ijk} \end{aligned} \quad (1)$$

where $O_{3,ijk}$, $HCHO_{ijk}$, $NO_{2_{ijk}}$, $TEMP_{ijk}$, SSR_{ijk}, RH_{ijk}, BLH_{ijk}, TCC_{ijk}, SP_{ijk}, and WS_{ijk} are surface-level O_3 concentration, TROPOMI HCHO, TROPOMI NO_2, temperature, surface net solar radiation, relative humidity, boundary layer height, total cloud cover, surface pressure, and wind speed on day k in grid cell j located in province i, respectively; $s_{1,i}$–$s_{8,i}$ and $\beta_{0,i}$ are the smoothing splines of each explanatory variable and the intercept in province i; $\varepsilon_{ijk} \sim N(0, \sigma_i)$ is an error term on day k in grid cell j located in province i. GAMs were constructed at the province level to align with the implementation of O_3 control

https://doi.org/10.5194/egusphere-2026-6618
Preprint. Discussion started: 16 November 2026
© Author(s) 2026. CC BY 4.0 License.

strategies in South Korea, thereby enhancing the practical applicability of the estimated regime thresholds (National Institute of Environmental Research (Nier), 2024a).

The HCHO/NO_2 level corresponding to the peak of the HCHO/NO_2 smoothing spline (i.e., $s_{1,i}$) was defined as the O_3 photochemical regime threshold. The spline describes how surface O_3 level varies with HCHO/NO_2 while holding the meteorological effects constant. Its peak therefore represents the point where the precursor proportions are the most favorable for $P(O_3)$, corresponding to the transition in $P(O_3)$ sensitivity. Potential collinearity between HCHO/NO_2 and the meteorological variables was assessed using Pearson correlation coefficients (r) (Hastie, 2009). Strong collinearity could inflate the standard errors (SEs) of the HCHO/NO_2 smoothing splines and thereby increase uncertainty in the estimated regime thresholds (Daoud, 2017; Wilks, 2011). However, all absolute correlation coefficients were <0.5 across the provinces, indicating that collinearity did not substantially impede threshold estimation.

2.5 Machine learning for identifying regime thresholds

A machine learning model rooted in boosting tree algorithms, eXtreme Gradient Boosting (XGBoost) (Chen and Guestrin, 2016), was used with SHapley Additive exPlanation (SHAP) to determine the O_3 photochemical regime thresholds (Lundberg and Lee, 2017). While effectively capturing complex non-linear relationships and interactions, XGBoost enabled precise adjustment for meteorological influences and yielded robust estimates of regime thresholds. In addition, XGBoost enables the use of HCHO and NO_2 as separate explanatory variables rather than relying on their ratio, which avoids structural bias induced by measurement errors in the ratio components (Tu et al., 2004; Bartlett and Partnoy, 2020). Hence, we considered XGBoost as a primary model. XGBoost models were trained by province using the same target and explanatory variables as those used in the GAMs, with HCHO and NO_2 included separately rather than as HCHO/NO_2. Model hyperparameters were optimized using the tree-structured Parzen estimator algorithm, a Bayesian optimization method implemented in Python package '*optuna*' (**Table S1**; **Text S1**).

$$O_{3,ijk} = XGB_i\begin{pmatrix} HCHO_{ijk},\ NO_{2_{ijk}},\ TEMP_{ijk},\ SSR_{ijk}, \\ RH_{ijk},\ BLH_{ijk},\ TCC_{ijk},\ SP_{ijk},\ WS_{ijk} \end{pmatrix} + \varepsilon_{ijk} \quad (2)$$

For the trained XGBoost models, SHAP was applied to quantify the contributions of each explanatory variable to surface-level O_3. TreeSHAP, a variant algorithm of SHAP for ensemble tree models implemented in the Python package '*shap*' (Lundberg et al., 2018), was applied to calculate SHAP values. Following the local accuracy property of SHAP, the model predictions for surface-level O_3 were expressed as the sum of the SHAP values of the explanatory variables and the base value (Zhang, 2025; Lundberg and Lee, 2017). The sum of the SHAP values for HCHO and NO_2 variables, denoted by ϕ^{chem}, was calculated to represent their combined contributions to O_3.

https://doi.org/10.5194/egusphere-2026-6618
Preprint. Discussion started: 16 November 2026
© Author(s) 2026. CC BY 4.0 License.

The O_3 photochemical regime thresholds were derived from the relationship between ϕ^{chem} and $HCHO/NO_2$. The two variables were paired for the same day and grid cell, and a cubic penalized B-spline was fitted with ϕ^{chem} as a target variable and $HCHO/NO_2$ as an explanatory variable (Eilers and Marx, 1996, 2010). The $HCHO/NO_2$ level corresponding to the spline peak was defined as the regime threshold, where the impact of $P(O_3)$ sensitivity on surface O_3 was maximized.

2.6 Model performance

The performances of the statistical and machine-learning models were evaluated using out-of-sample and out-of-grid 10-fold cross validation (CV) methods. In out-of-sample CV, all observations were randomly divided into 10 equal-sized subsets; each subset was used once for testing while the remaining nine subsets were used for training. Performance metrics, such as coefficient of determination (R^2), were calculated by comparing model estimates with measurements across the test sets (Hastie et al., 2009; Kohavi, 1995). In out-of-grid CV, grid cells rather than individual observations were randomly divided into 10 groups, and all observations from a given grid cell were assigned to the same fold. This approach evaluated model performance for grid cells without monitors (Childs et al., 2022; Tao et al., 2024). For the machine-learning models, nested CV was implemented by using the outer CV loop to evaluate model performance and an inner CV loop within each outer training fold to optimize hyperparameters. Restricting hyperparameter tuning to the outer training folds prevented information from the outer test folds from influencing model selection, thereby avoiding overly optimistic performance estimates (Cawley and Talbot, 2010).

2.7 Evaluation of uncertainty and spatial heterogeneity in regime thresholds

The sampling uncertainty and robustness of the regime thresholds derived from the GAM, XGBoost, and cubic polynomial approaches were evaluated using bootstrap resampling (Wilks, 2011; Efron, 1992). The cubic polynomial approach represents the conventional empirical approach described above, which was included as a reference method. Following previous research, the regime threshold was defined as the $HCHO/NO_2$ value corresponding to the peak of the cubic relationship between surface O_3 concentrations and satellite $HCHO/NO_2$ (Jin et al., 2020; Li et al., 2024; Ren et al., 2022; Ren et al., 2024). The bootstrap procedure involved: (1) resampling the equal-sized samples from the original dataset with replacement; (2) training the models to the resampled dataset; (3) estimating a regime threshold; (4) repeating steps (1)–(3) 500 times; and (5) calculating the SE as the sample standard deviation of the bootstrap thresholds (Hesterberg, 2015; Justus et al., 2024; Diciccio and Efron, 1996). The SE quantified the sampling uncertainty of the regime threshold, and the approximately normal bootstrap distribution justified calculating the 95% confidence interval (CI) as the sample estimate $\pm$ 1.96 × SE (Efron and Tibshirani, 1994).

To evaluate the spatial heterogeneity of the regime thresholds while accounting for province-specific sampling uncertainty, a random-effects meta-analysis was applied. This approach partitions the observed variation in regime threshold estimates into

https://doi.org/10.5194/egusphere-2026-6618
Preprint. Discussion started: 16 November 2026
© Author(s) 2026. CC BY 4.0 License.

sampling uncertainty and between-province heterogeneity. The pooled effect (θ) represents the mean regime threshold, while the between-province variance (τ^2) characterizes spatial heterogeneity across provinces (Harrer et al., 2021; Seabold and Perktold, 2010). The I^2 statistic indicates the proportion of the total variation attributable to spatial heterogeneity rather than sampling uncertainty (Higgins and Thompson, 2002).

2.8 O_3 response to NO_2 perturbation

The estimated regime thresholds were validated by examining whether they reasonably captured O_3 responses (i.e., increase or decrease) to NO_2 reductions. Specifically, a valid regime threshold should distinguish between opposite O_3 responses to NO_2 reductions, with O_3 decreasing under NO_x-limited or transitional conditions but increasing under NO_x-saturated conditions (Duncan et al., 2010). This perturbation-based evaluation is consistent with the conventional definition of O_3 sensitivity and has been widely applied using experiments and atmospheric chemistry models (Wu et al., 2022; Jung et al., 2022; Martin et al., 2004; Souri et al., 2026).

In the XGBoost model, the O_3 response and corresponding mean HCHO/NO_2 ratio were estimated for NO_2 reductions equivalent to n% of the province-specific mean NO_2 level, while all other explanatory variables were held constant:

$$y_{ijk}(n) = I\{XGB_i\left(\mathbf{x}^{\mathbb{X}}_{ijk} - \frac{n \cdot \overline{NO_{2_i}}}{200}\mathbf{e}_{NO_2}\right) - XGB_i\left(\mathbf{x}^{\mathbb{X}}_{ijk} + \frac{n \cdot \overline{NO_{2_i}}}{200}\mathbf{e}_{NO_2}\right) \geq 0\} \quad (3)$$

$$r_{ijk}(n) = \frac{1}{2} \cdot \left(\frac{HCHO_{ijk}}{NO_{2,ijk} - \frac{n \cdot \overline{NO_{2_i}}}{200}} + \frac{HCHO_{ijk}}{NO_{2,ijk} + \frac{n \cdot \overline{NO_{2_i}}}{200}}\right) \quad (4)$$

where $y_{ijk}(n)$ and $r_{ijk}(n)$ are the estimated O_3 response and mean HCHO/NO_2 ratio, respectively, under n% NO_2 reduction on day k in grid cell j located in province i; $\mathbf{x}^{\mathbb{X}}_{ijk}$, $NO_{2,ijk}$, and $HCHO_{ijk}$ are the observed vector of explanatory variables, TROPOMI NO_2 and TROPOMI HCHO, respectively, on day k in grid cell j located in province i; XGB_i and $\overline{NO_{2_i}}$ are the province-specific XGBoost model and mean NO_2 level in province i; $\mathbf{e}_{NO_2}$ is a unit vector that perturbs only the NO_2 component; and I is an indicator function that equals 1 if the specified condition is true and 0 otherwise.

For each province and NO_2 reduction scenario, a response-based split was identified from the relationship between $y_{ijk}(n)$ and $r_{ijk}(n)$ based on class-weighted Gini impurity (Breiman et al., 2017). The split for positive and negative O_3 responses was determined by minimizing Gini impurity, with inverse-frequency class weights applied to prevent the majority response class from dominating the split.

https://doi.org/10.5194/egusphere-2026-6618
Preprint. Discussion started: 16 November 2026
© Author(s) 2026. CC BY 4.0 License.

3 Results and Discussion

3.1 Summary statistics

The median of the daily surface-level O_3 concentration between 13:00 and 14:00 local time (daily 13–14h O_3) was 48.5 (25th–75th percentile = 38.0–61.5) ppb across 336 grid cells containing ground air quality monitors in South Korea for 2019–2023. The median of daily 13–14h O_3 varied annually from 46.5 ppb (2020) to 51.1 ppb (2023), monthly from 33.0 ppb (December) to 67.5 ppb (June), and by day of the week from 47.5 ppb (Monday) to 50.0 ppb (Saturday). The median of the daily grid-specific TROPOMI HCHO and NO_2 level (unit: $\times 10^{15}$ molecules/cm^2) was 9.06 (25th–75th percentile = 4.79–14.42) and 4.28 (25th–75th percentile = 2.61–7.62), respectively, showing a pronounced seasonal pattern with higher HCHO in the warm season and higher NO_2 in the cold season. Accordingly, the median of the grid-specific TROPOMI HCHO/NO_2 ratio was 1.90 (25th–75th percentile = 0.82–3.81) across 336 grid cells containing air quality monitors.

https://doi.org/10.5194/egusphere-2026-6618
Preprint. Discussion started: 16 November 2026
© Author(s) 2026. CC BY 4.0 License.

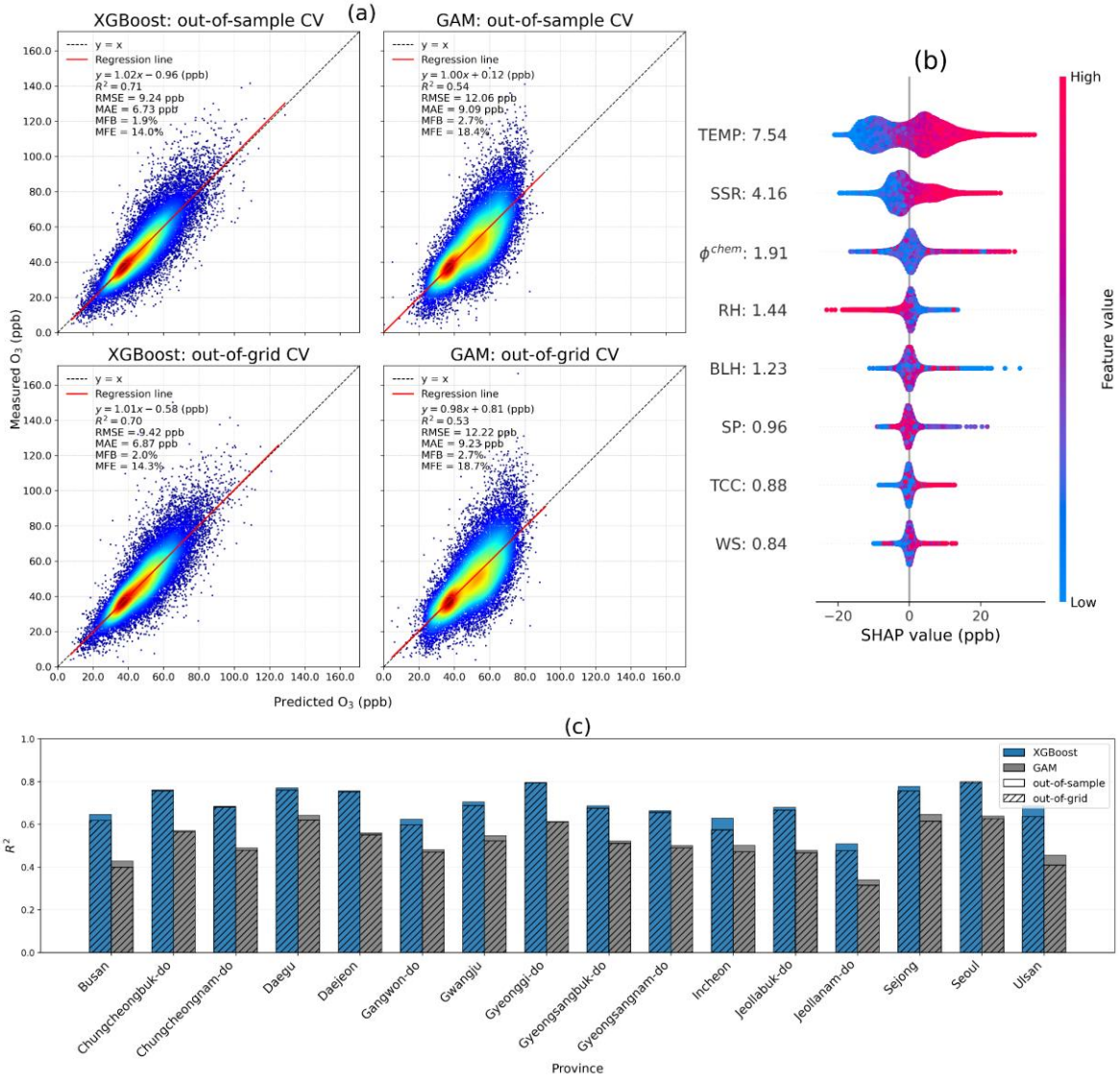


Figure 1. Model performances of XGBoost and GAMs evaluated by out-of-sample and out-of-grid 10-fold CV. In panel (a), all predicted and measured O_3 concentrations across 16 provinces in South Korea for 2019–2023 are compared. Panel (b) shows the contributions of the explanatory variables to the XGBoost model predictions, as quantified by SHAP values. The variables are ranked by their mean absolute SHAP values, with the corresponding values shown next to each variable. The R^2 values between predicted and measured O_3 concentrations are shown by province, model, and CV method in panel (c).

3.2 Model performance

The XGBoost models demonstrated reasonably high performance for surface-level O_3 prediction (**Fig. 1**a). Nested out-of-sample 10-fold CV yielded an overall R^2 of 0.71, with the province-specific R^2 values of 0.51–0.79 (**Fig. S1**), a mean

https://doi.org/10.5194/egusphere-2026-6618
Preprint. Discussion started: 16 November 2026
© Author(s) 2026. CC BY 4.0 License.

fractional bias (MFB) of 1.9%, and a mean fractional error (MFE) of 14.0% (Boylan and Russell, 2006). Nested out-of-grid 10-fold CV produced comparable results: an overall R^2 of 0.70, province-specific R^2 values of 0.48–0.80 (**Fig. S2**), an MFB of 2.0%, and an MFE of 14.3%. Province-specific R^2 values differed by less than 0.06 between the two CV methods (**Fig. 1**c), demonstrating stable predictive performance for unmonitored grid cells. This strong and spatially generalizable model performance suggests that the contributions of the explanatory variables closely reflect their real-world impacts on surface-level O_3 across South Korea. Specifically, TEMP and SSR were the two most influential variables, followed by ϕ^{chem} (mean rank = 3.6; SD = 0.81) and RH (mean rank = 4.3; SD = 1.35) (**Fig. 1**b; **Fig. S3**). Higher TEMP and SSR were associated with higher surface-level O_3 concentrations, whereas higher RH was associated with lower O_3, consistent with previously reported relationships (Bloomer et al., 2009; Xu et al., 2025; Coates et al., 2016; Oikonomakis et al., 2018; Guo et al., 2022; Yildizhan et al., 2024; Kavassalis and Murphy, 2017; Reddy et al., 2010).

The GAMs showed moderate predictive performance (**Fig. 1**a). Out-of-sample 10-fold CV yielded an overall R^2 of 0.54, province-specific R^2 values of 0.34–0.65 (**Fig. S4**), an MFB of 2.7%, and an MFE of 18.4%. Out-of-grid 10-fold CV demonstrated comparable performance: an overall R^2 of 0.53, province-specific R^2 values of 0.31–0.63 (**Fig. S5**), an MFB of 2.7%, and an MFE of 18.7%. Province-specific R^2 values differed by less than 0.05 between the CV methods (**Fig. 1**c), indicating spatially consistent performance despite the larger unexplained O_3 variability than in the XGBoost models. On the other hand, the province-level cubic polynomial model reasonably explained the binned relationship between O_3 and $HCHO/NO_2$ (R^2= 0.52–0.98). However, this model showed substantially lower predictive performance for daily observations (R^2= 0.009–0.152) relative to the XGBoost models and GAMs (**Table S2**).

https://doi.org/10.5194/egusphere-2026-6618
Preprint. Discussion started: 16 November 2026
© Author(s) 2026. CC BY 4.0 License.

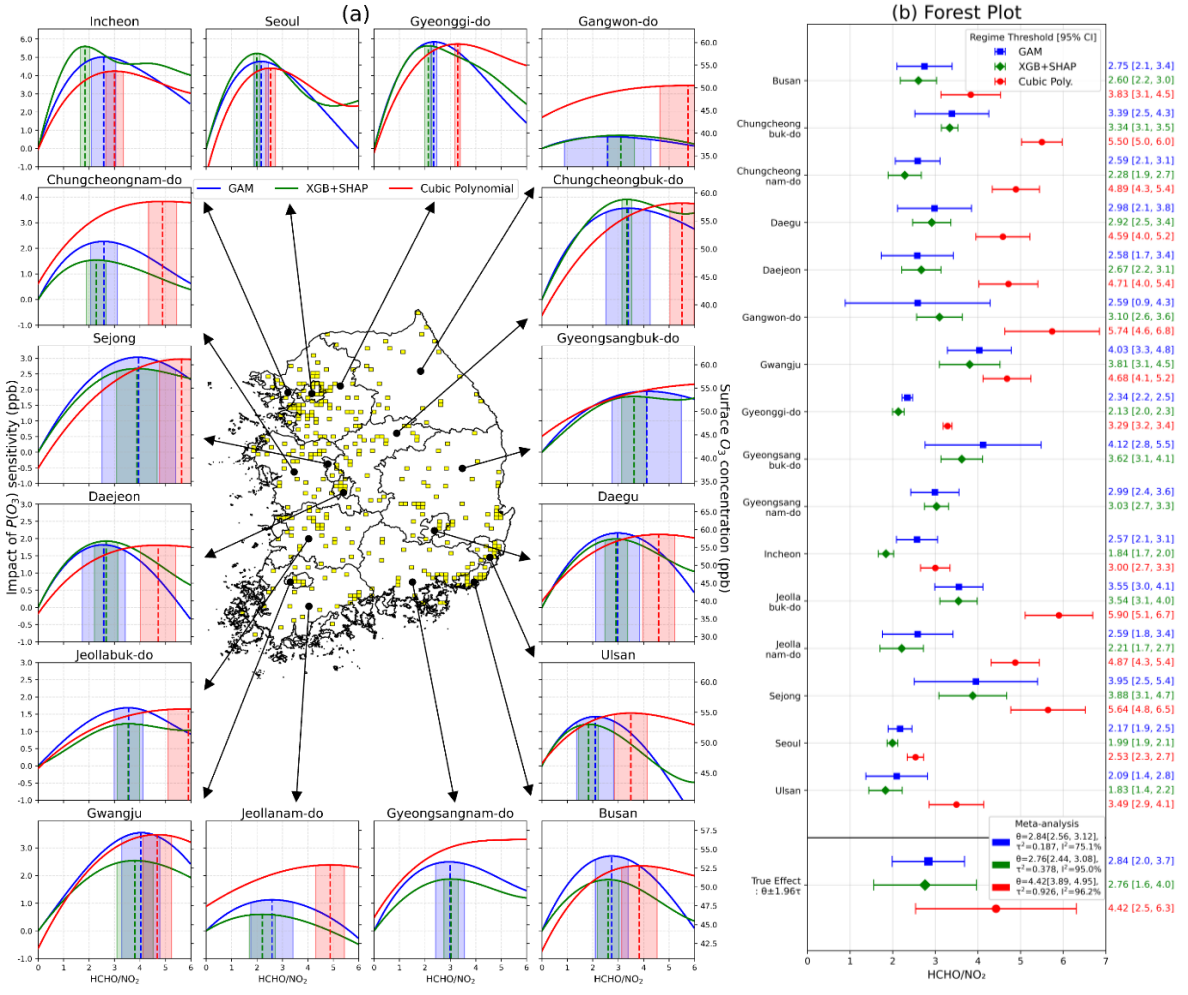


Figure 2. Estimated O_3 photochemical regime thresholds for 16 provinces using three empirical approaches: GAM, XGB+SHAP, and cubic polynomial. In panel (a), the solid curves show the estimated impacts of O_3 production sensitivity across the TROPOMI HCHO/NO_2 ratios by empirical approach and province. The vertical dashed lines indicate the regime thresholds, defined as the HCHO/NO_2 values at the curve peaks. The shaded ranges denote the bootstrap-based 95% CIs of the regime thresholds. The yellow squares on the map indicate grid cells containing urban or suburban air quality monitors. In panel (b), the province-specific regime thresholds and their 95% CIs are summarized using a random-effects meta-analysis. The symbols at the bottom of panel (b) indicate the pooled mean regime thresholds (θ), and the horizontal lines represent the corresponding 95% prediction intervals ($\theta \pm 1.96\tau$), which reflect between-province heterogeneity.

3.3 O_3 photochemical regime thresholds and spatial heterogeneity

Figure 2a shows the impacts of P(O_3) sensitivity on surface-level O_3 concentrations across the TROPOMI HCHO/NO_2 range using the three empirical approaches. The XGB+SHAP approach generally yielded the lowest province-specific

https://doi.org/10.5194/egusphere-2026-6618
Preprint. Discussion started: 16 November 2026
© Author(s) 2026. CC BY 4.0 License.

regime thresholds (1.8–3.9), followed by the GAM (2.1–4.1) and cubic polynomial approach (2.5–5.9). In Seoul, the capital city of South Korea, the XGB+SHAP regime threshold of 1.99 was consistent with the previously reported regime threshold of 1.8, which was derived from airborne measurements and a box-model simulation over Seoul in 2016 (Souri et al., 2020). This agreement contrasts with previous studies in which regime thresholds estimated using the conventional cubic polynomial approach diverged from atmospheric chemistry model estimates for the same regions (e.g., Los Angeles, California, U.S.) (Duncan et al., 2010; Jin et al., 2020; Jin et al., 2025). The cubic polynomial approach did not identify regime thresholds in Gyeongsangbuk-do and Gyeongsangnam-do because the fitted curves describing the effects of $P(O_3)$ sensitivity on O_3 increased monotonically and exhibited no peaks. This limitation was also reported previously (Jin et al., 2020). In contrast, the GAM and XGB+SHAP identified transition points in both provinces after accounting for meteorological variability, suggesting that the monotonic patterns were driven by meteorological conditions favorable for O_3 accumulation rather than by precursor proportions favorable for $P(O_3)$. These findings demonstrate that accounting for meteorological impacts is essential for identifying physically meaningful regime thresholds and further support the reliability of the GAM and XGB+SHAP approaches.

In **Fig. 2**a, the 95% CIs of the regime thresholds were interpreted as transitional regimes between NO_x-limited and NO_x-saturated regimes because the sampling uncertainty in the estimated regime thresholds could alter regime classification (Duncan et al., 2010). The 95% CIs were generally the narrowest for XGB+SHAP, intermediate for the cubic polynomial approach, and the widest for GAM, with the mean SEs of 0.21 (SD = 0.10), 0.32 (SD = 0.13), and 0.40 (SD = 0.21), respectively (**Fig. 2**b). Thus, XGB+SHAP represented the most robust regime thresholds, with a 34% lower mean SE than the conventional cubic polynomial approach. The greater uncertainty in the GAM and cubic polynomial approach likely resulted from their larger unexplained O_3 variability, caused by oversimplifying the effects of $P(O_3)$ sensitivity and meteorology in the GAM and by neglecting meteorological variability in the cubic polynomial. Greater unexplained variability increases the sensitivity of model estimates to resampling, thus widening the 95% CIs of the regime threshold estimates (Freedman, 1981; Wood, 2017; Breiman, 1996b, a).

As shown in the forest plot in **Fig. 2**b, the pooled mean regime thresholds estimated by the GAM and XGB+SHAP approaches were similar, at 2.84 (95% CI = 2.56–3.12) and 2.76 (95% CI = 2.44–3.08), respectively. Both thresholds were significantly lower than the threshold estimated from the cubic polynomial approach (4.42; 95% CI = 3.89–4.95). The 95% prediction interval was also substantially wider for the cubic polynomial approach (2.5–6.3) than for the GAM (2.0–3.7) and XGB+SHAP (1.6–4.0), indicating greater between-province heterogeneity when meteorological variability was not considered. This spatial heterogeneity likely reflects province-specific meteorological effects on surface-level O_3, which introduced additional variability into the cubic polynomial thresholds, whereas the GAM and XGB+SHAP reduced this influence by adjusting for meteorological variables.

https://doi.org/10.5194/egusphere-2026-6618
Preprint. Discussion started: 16 November 2026
© Author(s) 2026. CC BY 4.0 License.

These findings did not support a unified regime threshold across South Korea. Even for the GAM, showing the lowest between-province heterogeneity, an I^2 value above 75% indicated that most variation in the estimated regime thresholds was attributed to spatial heterogeneity rather than sampling uncertainty (Harrer et al., 2021). Therefore, province-specific regime thresholds are more appropriate for classifying O_3 photochemical regimes in South Korea. This heterogeneity may reflect regional O_3 formation characteristics not fully captured by the models, including differences in VOC reactivity and HCHO yields among the provinces.

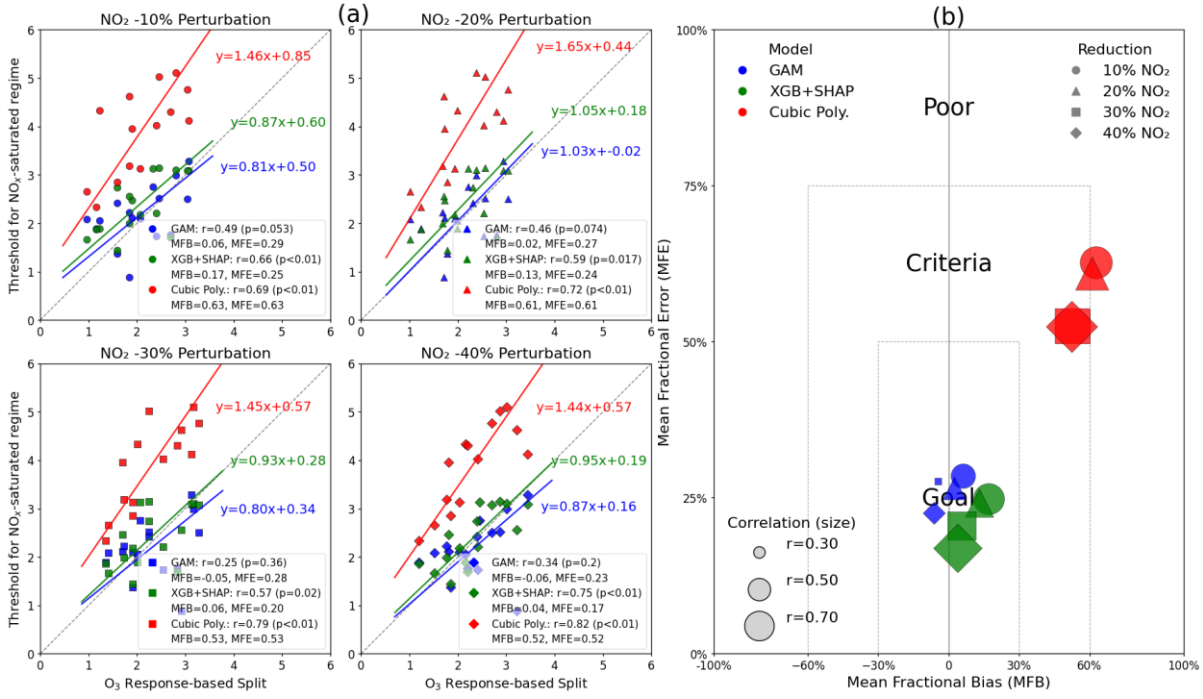


Figure 3. Comparison of the O_3 response-based splits under 10–40% NO_2 reduction scenarios with the thresholds for NO_x-saturated regime derived from the three empirical approaches across 16 provinces. In panel (a), the O_3 response-based splits for 16 provinces are compared to the thresholds for NO_x-saturated regime for each NO_2 reduction scenario. The colored straight lines represent total least-squares regression fits. Panel (b) summarizes the agreement between the response-based splits and the thresholds for NO_x-saturated regime across the modeling approaches and reduction scenarios. The ranges labeled "goal", "criteria", and "poor" indicate approximate levels of agreement based on Boylan and Russell (2006).

3.4 Validation of O_3 photochemical regime thresholds

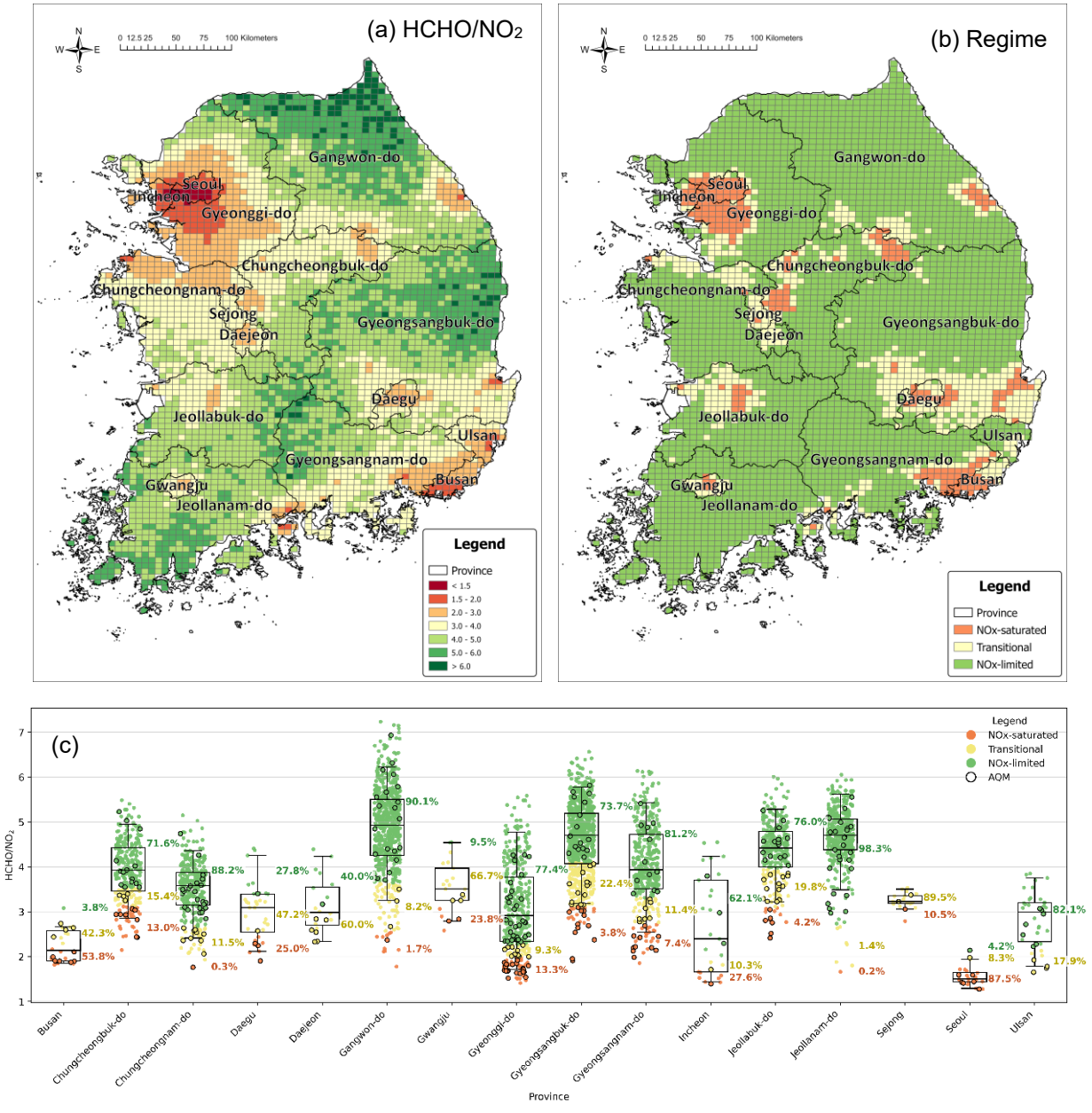
The O_3 photochemical regime thresholds were evaluated for their capability to capture the O_3 responses to different levels of NO_2 reduction. **Figure 3**a compares the response-based splits with the thresholds for the NO_x-saturated regime, defined as the lower boundaries of the transitional regime in **Fig. 2**, derived from the three empirical approaches. The total least-squares regression fits lying close to the 1:1 line suggest strong agreement between the response-based splits and the thresholds for

https://doi.org/10.5194/egusphere-2026-6618
Preprint. Discussion started: 16 November 2026
© Author(s) 2026. CC BY 4.0 License.

the NO_x-saturated regime (Markovsky and Van Huffel, 2007), implying that the province-specific regime thresholds effectively captured the O_3 response characteristics. In addition, as shown in **Fig. S6**, the O_3 response probabilities and O_3 response-based splits were estimated under the 10–40% NO_2 reduction scenarios by province. With increasing HCHO/NO_2, the probability of a decreasing O_3 response to NO_2 reduction ($y_{ijk}(n) = 0$) increased, while the probability of an increasing response ($y_{ijk}(n) = 1$) decreased. The response-based splits marked the point where the probabilities of increasing and decreasing O_3 responses were approximately equal, indicating a transition in O_3 response.

Figure 3b demonstrates that the NO_x-saturated regime thresholds estimated using the XGB+SHAP agreed more closely with the response-based splits than those estimated from the GAM and cubic polynomial approaches across all NO_2 reduction scenarios. The GAM and XGB+SHAP achieved agreement within the "goal" (agreement close to the best achievable) range for all NO_2 reduction scenarios, whereas the cubic polynomial approach fell within the "poor" (large disagreement for practical application) or "criteria" (acceptable agreement) ranges (Boylan and Russell, 2006). This contrast suggests that accounting for meteorological impacts improves agreement between the regime thresholds and O_3 responses. When comparing the GAM and XGB+SHAP results, the XGB+SHAP framework exhibited significant linear relationships between the response-based splits and the thresholds for the NO_x-saturated regime ($r = 0.57–0.75$, $p < 0.05$), whereas the GAM showed non-significant linear relationships for all NO_2 reduction scenarios ($r = 0.25–0.49$, $p > 0.05$). This finding demonstrates that the regime thresholds derived from the XGB+SHAP framework effectively captured not only the overall O_3 responses but also the between-province variations in O_3 response patterns. Consequently, our findings suggest that the XGB+SHAP framework provided the most robust regime thresholds, making it the most appropriate approach for identifying regional O_3 photochemical regimes.

https://doi.org/10.5194/egusphere-2026-6618
Preprint. Discussion started: 16 November 2026
© Author(s) 2026. CC BY 4.0 License.



330 **Figure 4.** Spatial distributions (5 km × 5 km) of (a) TROPOMI HCHO/NO_2 ratios and (b) O_3 photochemical regimes based on province-specific regime thresholds derived from the XGB+SHAP approach during the O_3 peak season (from April 15 to October 15) for 2019–2023. Panel (c) shows grid-specific distributions of TROPOMI HCHO/NO_2 ratios and O_3 photochemical regimes. The boxes indicate the interquartile ranges (25th–75th percentiles), with the horizontal lines within the boxes representing the medians and the whiskers extending to the 5th and 95th percentiles of HCHO/NO_2 ratios. The

https://doi.org/10.5194/egusphere-2026-6618
Preprint. Discussion started: 16 November 2026
© Author(s) 2026. CC BY 4.0 License.

percentages next to the boxes denote the proportions of grid cells classified into each regime. The black-outlined dots indicate grid cells containing ground air quality monitors.

3.5 Spatiotemporal distributions of HCHO/NO_2 and photochemical regimes

Figure 4a shows the spatial distributions of TROPOMI HCHO/NO_2 ratios during the O_3 peak season (from April 15 to October 15) for 2019–2023. The mean TROPOMI HCHO/NO_2 ratio across all grid cells was 4.17, ranging from 1.28 to 7.24. The Seoul Metropolitan Area (Seoul, Incheon, and Gyeonggi-do) and Busan (the second largest city by population) exhibited comparatively low HCHO/NO_2 ratios. This pattern was primarily attributable to high anthropogenic NO_x emissions (e.g., traffic) in densely populated areas. The relatively low HCHO/NO_2 ratios were also found in areas containing major industrial complexes (Kim and Lee, 2025). Conversely, the regions with low population density and large mountainous areas showed high HCHO/NO_2 ratios. For example, Gangwon-do had relatively few anthropogenic NO_x sources and extensive forests that likely emitted biogenic VOCs, which may have contributed to elevated HCHO/NO_2 ratios (Oak et al., 2025). During the O_3 non-peak season (from October 16 to April 14), the spatial distribution of HCHO/NO_2 was similar to that during the O_3 peak season, with relatively low values in highly populated and industrial areas (**Fig. S7**). However, the mean HCHO/NO_2 values (1.74; range = 0.27–5.48) were generally lower than those during the O_3 peak season, indicating a shift towards more NO_x-saturated regimes.

Figure 4b shows the regional photochemical regimes based on regional HCHO/NO_2 ratios and province-specific regime thresholds during the O_3 peak season. The regime thresholds derived using the XGB+SHAP approach were employed to classify the O_3 photochemical regimes because of their robustness. The Seoul Metropolitan Area, Busan, and other populated and industrial areas showed broad NO_x-saturated areas. Most other regions were in the NO_x-limited regime. During the O_3 non-peak season, the photochemical regimes were mostly NO_x-saturated or transitional, except for a few grid cells (**Fig. S7**). These seasonal contrasts suggest that season-specific O_3 control strategies may be more effective than a single year-round strategy. Month-to-month variations in HCHO/NO_2 ratios and their corresponding photochemical regimes are shown in **Fig. S8**.

Figure 4c shows the grid-specific distribution of HCHO/NO_2 ratios and their associated photochemical regimes by province during the O_3 peak season. The metropolitan cities of Seoul, Busan, and Gwangju predominantly showed NO_x-saturated or transitional regimes. Chungcheongbuk-do, Daegu, Gyeonggi-do, Gyeongsangnam-do, and Incheon included both NO_x-saturated and NO_x-limited areas. Spatially differentiated O_3 mitigation strategies, whenever feasible, can therefore help reduce O_3 air pollution effectively even in the same province. Finally, Chungcheongnam-do, Daejeon, Jeollanam-do, and Ulsan were classified as having transitional or NO_x-limited regimes. Our province-specific regime thresholds resulted in more extensive NO_x-saturated areas than those reported in an earlier study, which applied a uniform HCHO/NO_2 range of 1.0–2.5 to define the transitional regime across South Korea (Oak et al., 2025). The same conclusions were derived even

https://doi.org/10.5194/egusphere-2026-6618
Preprint. Discussion started: 16 November 2026
© Author(s) 2026. CC BY 4.0 License.

when applying the widely used transitional regime range of 1.0–2.0 that was proposed by Duncan et al. (2010). These more expanded NO_x-saturated areas provide a more plausible explanation for the nationwide increases in O_3 concentrations associated with NO_x reduction policies implemented in South Korea.

3.6 Limitations

This study has several limitations that need to be addressed in future work. First, the temporal coverage of this approach is limited to daily TROPOMI overpass time. This temporal constraint prevented us from capturing the diurnal patterns of $HCHO/NO_2$, regime thresholds, and $P(O_3)$ sensitivity (Jin et al., 2025), which are crucial for reflecting daily O_3 peaks that typically occur later in the afternoon. Although the current study focused on the spatial variability in O_3 photochemical regime thresholds using the TROPOMI retrievals, further studies incorporating more time-resolved satellite data, such as the Geostationary Environment Monitoring Spectrometer (GEMS, launched in 2020), can capture the diurnal patterns of HCHO and NO_2 (National Institute of Environmental Research (Nier), 2024c, b), and ultimately help meet air quality standards for maximum daily 8-hour average O_3 in South Korea (National Institute of Environmental Research (Nier), 2024a; Kim et al., 2021). Second, potential biases may exist in the empirical regime thresholds due to the uneven distribution of ground air quality monitors, which are disproportionately located in urban areas. Although we included suburban monitors and applied spatial CV methods to mitigate this potential bias, spatial imbalance persisted, and the validation ultimately relied on an unevenly distributed monitoring network. Accordingly, the empirical regime thresholds were likely to characterize O_3 photochemical regimes more accurately in urban areas, whereas rural regime classifications remain more uncertain. Third, TROPOMI HCHO data cannot fully capture regional VOC reactivity because HCHO yields vary by VOC species and depend on NO_x levels (Wolfe et al., 2016; Souri et al., 2023; Palmer et al., 2006; Chan Miller et al., 2017; Kang et al., 2023). To implicitly account for the spatial variability in HCHO yields, we estimated province-specific regime thresholds to reduce potential biases in regime classification. Nevertheless, this province-scale approach was insufficient to capture the variations in HCHO yields within individual provinces. Finally, the vertical profiles of HCHO and NO_2 may cause the column information to less accurately represent near-surface volume densities that are directly associated with $P(O_3)$ (Jin et al., 2020; Schroeder et al., 2017). Although this concern was mitigated by accounting for meteorological conditions, such as boundary layer height, which partially reflects the column-to-surface relationship (Jin et al., 2017; Arya, 1999), uncertainties related to the vertical representativeness of satellite columns were not fully characterized.

4 Conclusion

Our modeling framework provides an observation-based approach for characterizing O_3 photochemical regimes by deriving refined $HCHO/NO_2$ thresholds from integrated ground-based and satellite observations, while accounting for meteorological variability. The plausibility of the O_3 regime thresholds was supported by their agreement with response-based splits derived from model-estimated O_3 responses to NO_2 reductions. The derived thresholds had 34% lower mean SEs than those obtained

https://doi.org/10.5194/egusphere-2026-6618
Preprint. Discussion started: 16 November 2026
© Author(s) 2026. CC BY 4.0 License.

using the conventional cubic polynomial approach. A meta-analysis further demonstrated that a single nationwide threshold did not adequately represent regional differences in O_3 chemistry, whereas region-specific thresholds of 1.8–3.9 more reasonably characterized the O_3 production sensitivity. This framework proposes an empirical complement to atmospheric chemistry model-based approaches by using observed surface-level O_3 and satellite-derived HCHO and NO_2 without directly relying on emission inventories. Given the global availability of satellite HCHO and NO_2 retrievals, the framework requires only routine O_3 measurements from ground air quality monitors, making it applicable to many regions worldwide. Consequently, this study demonstrates the benefits of using satellite remote sensing and machine learning models for translating satellite-based indicators into observation-constrained diagnostics of surface-level O_3 photochemical regimes. This study can inform region-specific NO_x and VOC control strategies to effectively mitigate ambient O_3 air pollution and its associated health outcomes.

Data availability

The dataset used for investigating O_3 photochemical regimes is pubilcly available at https://zenodo.org/records/20192957.

Supplement link

The link to the supplement will be included by Copernicus, if applicable.

Author contributions

CK contributed to conceptualization and methodology development, performed the formal analysis and visualization, and wrote the original draft. **HJL** contributed to conceptualization and methodology development, supervised the study, and reviewed and edited the manuscript.

Competing interests

The authors declare that they have no conflicts of interest.

Acknowledgements

This work was supported by the National Research Foundation of Korea (NRF) grant funded by the Korean government (MSIT) in Grant No. RS-2026-25537812.

https://doi.org/10.5194/egusphere-2026-6618
Preprint. Discussion started: 16 November 2026
© Author(s) 2026. CC BY 4.0 License.

Review statement

The review statement will be added by Copernicus Publications listing the handling editor as well as all contributing referees according to their status anonymous or identified.

References

Acdan, J. J. M., Pierce, R. B., Dickens, A. F., Adelman, Z., and Nergui, T.: Examining TROPOMI formaldehyde to nitrogen dioxide ratios in the Lake Michigan region: implications for ozone exceedances, Atmos. Chem. Phys., 23, 7867-7885, 10.5194/acp-23-7867-2023, 2023.

Arya, S. P.: Air pollution meteorology and dispersion, Oxford University Press New York1999.

Bartlett, R. and Partnoy, F.: The ratio problem, Available at SSRN 3605606, 2020.

Bloomer, B. J., Stehr, J. W., Piety, C. A., Salawitch, R. J., and Dickerson, R. R.: Observed relationships of ozone air pollution with temperature and emissions, Geophys. Res. Lett., 36, 10.1029/2009GL037308, 2009.

Boersma, K. F., Eskes, H. J., Richter, A., De Smedt, I., Lorente, A., Beirle, S., Van Geffen, J. H. G. M., Zara, M., Peters, E., Van Roozendael, M., Wagner, T., Maasakkers, J. D., Van Der A, R. J., Nightingale, J., De Rudder, A., Irie, H., Pinardi, G., Lambert, J.-C., and Compernolle, S. C.: Improving algorithms and uncertainty estimates for satellite NO2 retrievals: results from the quality assurance for the essential climate variables (QA4ECV) project, Atmos. Meas. Tech., 11, 6651-6678, 10.5194/amt-11-6651-2018, 2018.

Boylan, J. W. and Russell, A. G.: PM and light extinction model performance metrics, goals, and criteria for three-dimensional air quality models, Atmos. Environ., 40, 4946-4959, 10.1016/j.atmosenv.2005.09.087, 2006.

Breiman, L.: Heuristics of instability and stabilization in model selection, Ann. Stat., 24, 2350-2383, 1996a.

Breiman, L.: Bagging predictors, Mach. Learn., 24, 123-140, 1996b.

Breiman, L., Friedman, J., Olshen, R. A., and Stone, C. J.: Classification and regression trees, Chapman and Hall/CRC2017.

Cawley, G. C. and Talbot, N. L.: On over-fitting in model selection and subsequent selection bias in performance evaluation, J. Mach. Learn. Res., 11, 2079-2107, 2010.

Chan Miller, C., Jacob, D. J., Marais, E. A., Yu, K., Travis, K. R., Kim, P. S., Fisher, J. A., Zhu, L., Wolfe, G. M., Hanisco, T. F., Keutsch, F. N., Kaiser, J., Min, K.-E., Brown, S. S., Washenfelder, R. A., González Abad, G., and Chance, K.: Glyoxal yield from isoprene oxidation and relation to formaldehyde: chemical mechanism, constraints from SENEX aircraft observations, and interpretation of OMI satellite data, Atmos. Chem. Phys., 17, 8725-8738, 10.5194/acp-17-8725-2017, 2017.

Chen, T. and Guestrin, C.: XGBoost, Proceedings of the 22nd ACM SIGKDD International Conference on Knowledge Discovery and Data Mining, 10.1145/2939672.2939785, 2016.

https://doi.org/10.5194/egusphere-2026-6618
Preprint. Discussion started: 16 November 2026
© Author(s) 2026. CC BY 4.0 License.

Childs, M. L., Li, J., Wen, J., Heft-Neal, S., Driscoll, A., Wang, S., Gould, C. F., Qiu, M., Burney, J., and Burke, M.: Daily Local-Level Estimates of Ambient Wildfire Smoke PM2.5 for the Contiguous US, Environ. Sci. Technol., 56, 13607-13621, 10.1021/acs.est.2c02934, 2022.

Coates, J., Mar, K. A., Ojha, N., and Butler, T. M.: The influence of temperature on ozone production under varying NOx conditions–a modelling study, Atmos. Chem. Phys., 16, 11601-11615, 2016.

Daoud, J. I.: Multicollinearity and Regression Analysis, Journal of Physics: Conference Series, 949, 012009, 10.1088/1742-6596/949/1/012009, 2017.

S5P/TROPOMI HCHO ATBD: https://sentinels.copernicus.eu/web/sentinel/copernicus/sentinel-5p, last access: 10 February 2026.

De Smedt, I., Theys, N., Yu, H., Danckaert, T., Lerot, C., Compernolle, S., Van Roozendael, M., Richter, A., Hilboll, A., Peters, E., Pedergnana, M., Loyola, D., Beirle, S., Wagner, T., Eskes, H., Van Geffen, J., Boersma, K. F., and Veefkind, P.: Algorithm theoretical baseline for formaldehyde retrievals from S5P TROPOMI and from the QA4ECV project, Atmos. Meas. Tech., 11, 2395-2426, 10.5194/amt-11-2395-2018, 2018.

DiCiccio, T. J. and Efron, B.: Bootstrap confidence intervals, Stat. Sci., 11, 189-228, 1996.

Duncan, B. N., Yoshida, Y., Olson, J. R., Sillman, S., Martin, R. V., Lamsal, L., Hu, Y., Pickering, K. E., Retscher, C., Allen, D. J., and Crawford, J. H.: Application of OMI observations to a space-based indicator of NOx and VOC controls on surface ozone formation, Atmos. Environ., 44, 2213-2223, 10.1016/j.atmosenv.2010.03.010, 2010.

Efron, B.: Bootstrap methods: another look at the jackknife, Breakthroughs in statistics: Methodology and distribution, Springer, 569-593 pp.1992.

Efron, B. and Tibshirani, R. J.: An introduction to the bootstrap, Chapman and Hall/CRC1994.

Eilers, P. H. C. and Marx, B. D.: Flexible smoothing with B-splines and penalties, Stat. Sci., 11, 89-121, 10.1214/ss/1038425655, 1996.

Eilers, P. H. C. and Marx, B. D.: Splines, knots, and penalties, WIREs Comp. Stat., 2, 637-653, 10.1002/wics.125, 2010.

Sentinel-5P TROPOMI Level-2 Product User Manual Nitrogen Dioxide: https://sentinels.copernicus.eu/web/sentinel/copernicus/sentinel-5p, last access: 10 February 2026.

Sentinel-5 Precursor Level 2 Formaldehyde: https://sentinels.copernicus.eu/data-products/-/asset_publisher/fp37fc19FN8F/content/sentinel-5-precursor-level-2-formaldehyde, last access: 27 June 2024.

Sentinel-5 Precursor Level 2 Nitrogen Dioxide: https://sentinels.copernicus.eu/data-products/-/asset_publisher/fp37fc19FN8F/content/sentinel-5-precursor-level-2-nitrogen-dioxide, last access: 27 June 2024.

Freedman, D. A.: Bootstrapping regression models, Ann. Stat., 1218-1228, 1981.

Guo, B., Wu, H., Pei, L., Zhu, X., Zhang, D., Wang, Y., and Luo, P.: Study on the spatiotemporal dynamic of ground-level ozone concentrations on multiple scales across China during the blue sky protection campaign, Environ. Int., 170, 107606, 10.1016/j.envint.2022.107606, 2022.

https://doi.org/10.5194/egusphere-2026-6618
Preprint. Discussion started: 16 November 2026
© Author(s) 2026. CC BY 4.0 License.

Harrer, M., Cuijpers, P., Furukawa, T. A., and Ebert, D. D.: Doing Meta-Analysis With R: A Hands-On Guide, 1st, Chapman & Hall/CRC Press, Boca Raton, FL and London2021.

Hastie, T.: The elements of statistical learning: data mining, inference, and prediction, springer2009.

Hastie, T. and Tibshirani, R.: Generalized additive models, Stat. Sci., 1, 297-310, 1986.

Hastie, T., Tibshirani, R., and Friedman, J.: The elements of statistical learning, Springer series in statistics New-York2009.

Hastie, T. J.: Generalized additive models, Statistical models in S, 249-307, 2017.

ERA5 hourly data on single levels from 1940 to present: https://cds.climate.copernicus.eu/datasets/reanalysis-era5-single-levels?tab=overview, last access: 11 May 2025.

Hesterberg, T. C.: What teachers should know about the bootstrap: Resampling in the undergraduate statistics curriculum, The american statistician, 69, 371-386, 2015.

Higgins, J. P. and Thompson, S. G.: Quantifying heterogeneity in a meta-analysis, Stat. Med., 21, 1539-1558, 2002.

Jin, X., Fiore, A., Boersma, K. F., Smedt, I., and Valin, L.: Inferring Changes in Summertime Surface Ozone-NOx-VOC Chemistry over U.S. Urban Areas from Two Decades of Satellite and Ground-Based Observations, Environ. Sci. Technol., 54, 6518-6529, 10.1021/acs.est.9b07785, 2020.

Jin, X., Yang, Y., Gonzalez Abad, G., Nowlan, C., and Liu, X.: Observing the Diurnal Variations of Ozone-NOx-VOC Chemistry Over the U.S. From the Geostationary TEMPO Instrument, Geophys. Res. Lett., 52, 10.1029/2025gl116394, 2025.

Jin, X., Fiore, A. M., Murray, L. T., Valin, L. C., Lamsal, L. N., Duncan, B., Boersma, K. F., De Smedt, I., Abad, G. G., Chance, K., and Tonnesen, G. S.: Evaluating a Space-Based Indicator of Surface Ozone-NOx-VOC Sensitivity Over Midlatitude Source Regions and Application to Decadal Trends, J. Geophys. Res.-Atmos., 122, 10-461, 10.1002/2017JD026720, 2017.

Johnson, M. S., Souri, A. H., Philip, S., Kumar, R., Naeger, A., Geddes, J., Judd, L., Janz, S., Chong, H., and Sullivan, J.: Satellite remote-sensing capability to assess tropospheric-column ratios of formaldehyde and nitrogen dioxide: case study during the Long Island Sound Tropospheric Ozone Study 2018 (LISTOS 2018) field campaign, Atmos. Meas. Tech., 16, 2431-2454, 10.5194/amt-16-2431-2023, 2023.

Jung, J., Choi, Y., Mousavinezhad, S., Kang, D., Park, J., Pouyaei, A., Ghahremanloo, M., Momeni, M., and Kim, H.: Changes in the ozone chemical regime over the contiguous United States inferred by the inversion of NOx and VOC emissions using satellite observation, Atmos. Res., 270, 1-14, 10.1016/j.atmosres.2022.106076, 2022.

Justus, V. L., Rodrigues, V. B., and Sousa, A. R. d. S.: Bootstrap confidence intervals: A comparative simulation study, arXiv preprint arXiv:2404.12967, 2024.

Kang, Y., Tang, G., Li, Q., Liu, B., Yao, D., Wang, Y., Wang, Y., Wang, Y., and Liu, W.: Problems with and Improvement of HCHO/NO2 for Diagnosing Ozone Sensitivity—A Case in Beijing, Remote Sensing, 15, 1982, 10.3390/rs15081982, 2023.

Kavassalis, S. C. and Murphy, J. G.: Understanding ozone-meteorology correlations: A role for dry deposition, Geophys. Res. Lett., 44, 2922-2931, 2017.

https://doi.org/10.5194/egusphere-2026-6618
Preprint. Discussion started: 16 November 2026
© Author(s) 2026. CC BY 4.0 License.

Keller, C. A., Knowland, K. E., Duncan, B. N., Liu, J., Anderson, D. C., Das, S., Lucchesi, R. A., Lundgren, E. W., Nicely, J. M., Nielsen, E., Ott, L. E., Saunders, E., Strode, S. A., Wales, P. A., Jacob, D. J., and Pawson, S.: Description of the NASA GEOS Composition Forecast Modeling System GEOS-CF v1.0, J. Adv. Model. Earth Syst., 13, 10.1029/2020ms002413, 2021.

Kim, J., Lee, J., Han, J.-S., Choi, J., Kim, D.-G., Park, J., and Lee, G.: Long-term Assessment of Ozone Nonattainment Changes in South Korea Compared to US, and EU Ozone Guidelines, Asian J. Atmos. Environ., 15, 20-32, 10.5572/ajae.2021.098, 2021.

Kim, N. R. and Lee, H. J.: Leveraging High-Resolution Satellite-Derived NO2 Estimates to Evaluate NO2 Exposure Representativeness and Socioeconomic Disparities, Environ. Sci. Technol., 59, 3434-3442, 10.1021/acs.est.4c10996, 2025.

Kleinman, L. I.: The dependence of tropospheric ozone production rate on ozone precursors, Atmos. Environ., 39, 575-586, 10.1016/j.atmosenv.2004.08.047, 2005.

Kleinman, L. I., Daum, P. H., Lee, Y. N., Nunnermacker, L. J., Springston, S. R., Weinstein-Lloyd, J., and Rudolph, J.: Sensitivity of ozone production rate to ozone precursors, Geophys. Res. Lett., 28, 2903-2906, 10.1029/2000gl012597, 2001.

Kleinman, L. I., Daum, P. H., Lee, J. H., Lee, Y. N., Nunnermacker, L. J., Springston, S. R., Newman, L., Weinstein-Lloyd, J., and Sillman, S.: Dependence of ozone production on NO and hydrocarbons in the troposphere, Geophys. Res. Lett., 24, 2299-2302, 10.1029/97gl02279, 1997.

Kohavi, R.: A study of cross-validation and bootstrap for accuracy estimation and model selection, International Joint Conference on Artificial Intelligence1995.

Ground-level hourly ozone data: https://www.airkorea.or.kr/web/, last access: 21 May 2025.

Open MET data Portal: https://data.kma.go.kr/cmmn/main.do, last access: 31 March 2025.

Kusumaningtyas, S. D. A., Tonokura, K., Muharsyah, R., Gunawan, D., Sopaheluwakan, A., Iriana, W., Lestari, P., Permadi, D. A., Rahmawati, R., and Samputra, N. A. R.: Comprehensive analysis of long-term trends, meteorological influences, and ozone formation sensitivity in the Jakarta Greater Area, Sci Rep, 14, 10.1038/s41598-024-60374-2, 2024.

Lee, H. J., Kuwayama, T., and FitzGibbon, M.: Trends of ambient O3 levels associated with O3 precursor gases and meteorology in California: Synergies from ground and satellite observations, Remote Sens. Environ., 284, 10.1016/j.rse.2022.113358, 2023.

Li, J., Cai, J., Zhang, M., Liu, H., Han, X., Cai, X., and Xu, Y.: Model analysis of meteorology and emission impacts on springtime surface ozone in Shandong, Sci. Total Environ., 771, 144784, 10.1016/j.scitotenv.2020.144784, 2021.

Li, T., Zhang, Q., Peng, Y., Guan, X., Li, L., Mu, J., Wang, X., Yin, X., and Wang, Q.: Contributions of various driving factors to air pollution events: Interpretability analysis from Machine learning perspective, Environ. Int., 173, 107861, 10.1016/j.envint.2023.107861, 2023.

Li, Y., Yu, C., Tao, J., Lu, X., and Chen, L.: Analysis of Ozone Formation Sensitivity in Chinese Representative Regions Using Satellite and Ground-Based Data, Remote Sensing, 16, 316, 10.3390/rs16020316, 2024.

https://doi.org/10.5194/egusphere-2026-6618
Preprint. Discussion started: 16 November 2026
© Author(s) 2026. CC BY 4.0 License.

Lundberg, S. M. and Lee, S.-I.: A unified approach to interpreting model predictions, Advances in neural information processing systems2017.

Lundberg, S. M., Erion, G. G., and Lee, S.-I.: Consistent individualized feature attribution for tree ensembles, arXiv preprint arXiv:1802.03888, 2018.

Markovsky, I. and Van Huffel, S.: Overview of total least-squares methods, Signal Process., 87, 2283-2302, 2007.

Martin, R. V., Fiore, A. M., and Van Donkelaar, A.: Space-based diagnosis of surface ozone sensitivity to anthropogenic emissions, Geophys. Res. Lett., 31, 10.1029/2004gl019416, 2004.

ERA5-Land hourly data from 1950 to present: https://cds.climate.copernicus.eu/datasets/reanalysis-era5-land?tab=overview, last access: 11 May 2025.

Annual Report of Air Quality In Korea 2023: https://www.me.go.kr/home/web/main.do, last access: 10 June 2024.

Algorithm Theoretical Basis Document: NO2 Retrieval Algorithm https://nesc.nier.go.kr/en/html/index.do, last access: 18 January 2026.

Algorithm Theoretical Basis Document: VOC (HCHO/CHOCHO) Retrieval Algorithm https://nesc.nier.go.kr/en/html/index.do, last access: 18 January 2026.

Oak, Y. J., Jacob, D. J., Pendergrass, D. C., Dang, R., Colombi, N. K., Chong, H., Lee, S., Kuk, S. K., and Kim, J.: Air quality trends and regimes in South Korea inferred from 2015–2023 surface and satellite observations, Atmos. Chem. Phys., 25, 3233-3252, 10.5194/acp-25-3233-2025, 2025.

Oikonomakis, E., Aksoyoglu, S., Wild, M., Ciarelli, G., Baltensperger, U., and Prévôt, A. S. H.: Solar "brightening" impact on summer surface ozone between 1990 and 2010 in Europe – a model sensitivity study of the influence of the aerosol–radiation interactions, Atmos. Chem. Phys., 18, 9741-9765, 10.5194/acp-18-9741-2018, 2018.

Palmer, P. I., Abbot, D. S., Fu, T. M., Jacob, D. J., Chance, K., Kurosu, T. P., Guenther, A., Wiedinmyer, C., Stanton, J. C., Pilling, M. J., Pressley, S. N., Lamb, B., and Sumner, A. L.: Quantifying the seasonal and interannual variability of North American isoprene emissions using satellite observations of the formaldehyde column, J. Geophys. Res.-Atmos., 111, 10.1029/2005jd006689, 2006.

Pedersen, E. J., Miller, D. L., Simpson, G. L., and Ross, N.: Hierarchical generalized additive models in ecology: an introduction with mgcv, PeerJ, 7, e6876, 10.7717/peerj.6876, 2019.

Reddy, B. S. K., Kumar, K. R., Balakrishnaiah, G., Gopal, K. R., Reddy, R. R., Ahammed, Y. N., Narasimhulu, K., Reddy, L. S. S., and Lal, S.: Observational studies on the variations in surface ozone concentration at Anantapur in southern India, Atmos. Res., 98, 125-139, 10.1016/j.atmosres.2010.06.008, 2010.

Ren, J., Guo, F., and Xie, S.: Diagnosing ozone–NOx–VOC sensitivity and revealing causes of ozone increases in China based on 2013–2021 satellite retrievals, Atmos. Chem. Phys., 22, 15035-15047, 10.5194/acp-22-15035-2022, 2022.

Ren, J., Hao, Y., Zheng, X., Li, X., and Xie, S.: Ozone response to precursors changes in the Chengdu-Chongqing economic circle, China, from satellite and ground-based observations, Sci. Total Environ., 953, 176037, 10.1016/j.scitotenv.2024.176037, 2024.

https://doi.org/10.5194/egusphere-2026-6618
Preprint. Discussion started: 16 November 2026
© Author(s) 2026. CC BY 4.0 License.

Sentinel-5P Level 2 Product User Manual Formaldehyde HCHO: https://sentinels.copernicus.eu/web/sentinel/copernicus/sentinel-5p, last access: 10 February 2026.

Schroeder, J. R., Crawford, J. H., Fried, A., Walega, J., Weinheimer, A., Wisthaler, A., Müller, M., Mikoviny, T., Chen, G., Shook, M., Blake, D. R., and Tonnesen, G. S.: New insights into the column CH2O/NO2 ratio as an indicator of near-surface ozone sensitivity, J. Geophys. Res.-Atmos., 122, 8885-8907, 10.1002/2017jd026781, 2017.

Seabold, S. and Perktold, J.: Statsmodels: econometric and statistical modeling with python, SciPy, 7, 92-96, 2010.

Seinfeld, J. H. and Pandis, S. N.: Atmospheric chemistry and physics: from air pollution to climate change, John Wiley & Sons2016.

pyGAM: Generalized Additive Models in Python: https://doi.org/10.5281/zenodo.1208723, last access: 17 February 2025.

Shin, M. Y. and Lee, H. J.: A comprehensive multi-tiered approach to assessing weather penalties on O(3) levels and exceedance days in Seoul using generalized additive models (2001-2019), Chemosphere, 368, 143687, 10.1016/j.chemosphere.2024.143687, 2024.

Sillman, S.: The relation between ozone, NOx and hydrocarbons in urban and polluted rural environments, Atmos. Environ., 33, 1821-1845, 1999.

Sillman, S. and He, D.: Some theoretical results concerning O3-NOx-VOC chemistry and NOx-VOC indicators, J. Geophys. Res.-Atmos., 107, 10.1029/2001jd001123, 2002.

Silvern, R. F., Jacob, D. J., Mickley, L. J., Sulprizio, M. P., Travis, K. R., Marais, E. A., Cohen, R. C., Laughner, J. L., Choi, S., Joiner, J., and Lamsal, L. N.: Using satellite observations of tropospheric NO2 columns to infer long-term trends in US NOx emissions: the importance of accounting for the free tropospheric NO2 background, Atmos. Chem. Phys., 19, 8863-8878, 10.5194/acp-19-8863-2019, 2019.

Souri, A. H., González Abad, G., Duncan, B. N., and Oman, L. D.: Beyond binary maps from HCHO/NO2: a deep neural network approach to global daily mapping of net ozone production rates and sensitivities constrained by satellite observations (2005–2023), Atmos. Chem. Phys., 26, 809-837, 10.5194/acp-26-809-2026, 2026.

Souri, A. H., Nowlan, C. R., Wolfe, G. M., Lamsal, L. N., Miller, C. E. C., Abad, G. G., Janz, S. J., Fried, A., Blake, D. R., Weinheimer, A. J., Diskin, G. S., Liu, X., and Chance, K.: Revisiting the effectiveness of HCHO/NO2 ratios for inferring ozone sensitivity to its precursors using high resolution airborne remote sensing observations in a high ozone episode during the KORUS-AQ campaign, Atmos. Environ., 224, 10.1016/j.atmosenv.2020.117341, 2020.

Souri, A. H., Johnson, M. S., Wolfe, G. M., Crawford, J. H., Fried, A., Wisthaler, A., Brune, W. H., Blake, D. R., Weinheimer, A. J., Verhoelst, T., Compernolle, S., Pinardi, G., Vigouroux, C., Langerock, B., Choi, S., Lamsal, L., Zhu, L., Sun, S., Cohen, R. C., Min, K.-E., Cho, C., Philip, S., Liu, X., and Chance, K.: Characterization of errors in satellite-based HCHO/NO2 tropospheric column ratios with respect to chemistry, column-to-PBL translation, spatial representation, and retrieval uncertainties, Atmos. Chem. Phys., 23, 1963-1986, 10.5194/acp-23-1963-2023, 2023.

https://doi.org/10.5194/egusphere-2026-6618
Preprint. Discussion started: 16 November 2026
© Author(s) 2026. CC BY 4.0 License.

Tao, C., Peng, Y., Zhang, Q., Zhang, Y., Gong, B., Wang, Q., and Wang, W.: Diagnosing ozone–NOx–VOC–aerosol sensitivity and uncovering causes of urban–nonurban discrepancies in Shandong, China, using transformer-based estimations, Atmos. Chem. Phys., 24, 4177-4192, 10.5194/acp-24-4177-2024, 2024.

Tu, Y.-K., Clerehugh, V., and Gilthorpe, M. S.: Ratio variables in regression analysis can give rise to spurious results: illustration from two studies in periodontology, J. Dent., 32, 143-151, 10.1016/j.jdent.2003.09.004, 2004.

TROPOMI ATBD of the total and tropospheric NO2 data products: https://sentinels.copernicus.eu/web/sentinel/copernicus/sentinel-5p, last access: 10 January 2026.

Wang, K., Yahya, K., Zhang, Y., Hogrefe, C., Pouliot, G., Knote, C., Hodzic, A., San Jose, R., Perez, J. L., and Jiménez-Guerrero, P.: A multi-model assessment for the 2006 and 2010 simulations under the Air Quality Model Evaluation International Initiative (AQMEII) Phase 2 over North America: Part II. Evaluation of column variable predictions using satellite data, Atmos. Environ., 115, 587-603, 2015.

Wang, L., Chen, B., Ouyang, J., Mu, Y., Zhen, L., Yang, L., Xu, W., and Tang, L.: Causal-inference machine learning reveals the drivers of China's 2022 ozone rebound, Env. Sci. Ecotechnol., 24, 100524, 10.1016/j.ese.2025.100524, 2025.

Wang, W., Van Der A, R., Ding, J., Van Weele, M., and Cheng, T.: Spatial and temporal changes of the ozone sensitivity in China based on satellite and ground-based observations, Atmos. Chem. Phys., 21, 7253-7269, 10.5194/acp-21-7253-2021, 2021.

Whalley, L. K., Slater, E. J., Woodward-Massey, R., Ye, C., Lee, J. D., Squires, F., Hopkins, J. R., Dunmore, R. E., Shaw, M., Hamilton, J. F., Lewis, A. C., Mehra, A., Worrall, S. D., Bacak, A., Bannan, T. J., Coe, H., Percival, C. J., Ouyang, B., Jones, R. L., Crilley, L. R., Kramer, L. J., Bloss, W. J., Vu, T., Kotthaus, S., Grimmond, S., Sun, Y., Xu, W., Yue, S., Ren, L., Acton, W. J. F., Hewitt, C. N., Wang, X., Fu, P., and Heard, D. E.: Evaluating the sensitivity of radical chemistry and ozone formation to ambient VOCs and NOx in Beijing, Atmos. Chem. Phys., 21, 2125-2147, 10.5194/acp-21-2125-2021, 2021.

Wilks, D. S.: Statistical methods in the atmospheric sciences, Academic press2011.

Wolfe, G. M., Kaiser, J., Hanisco, T. F., Keutsch, F. N., de Gouw, J. A., Gilman, J. B., Graus, M., Hatch, C. D., Holloway, J., Horowitz, L. W., Lee, B. H., Lerner, B. M., Lopez-Hilifiker, F., Mao, J., Marvin, M. R., Peischl, J., Pollack, I. B., Roberts, J. M., Ryerson, T. B., Thornton, J. A., Veres, P. R., and Warneke, C.: Formaldehyde production from isoprene oxidation across NOx regimes, Atmos. Chem. Phys., 16, 2597-2610, 10.5194/acp-16-2597-2016, 2016.

Wood, S. N.: Generalized Additive Models an introduction with R, Chapman and Hall/CRC, New York, https://doi.org/10.1201/9781315370279, 2017.

Wu, S., Lee, H. J., Anderson, A., Liu, S., Kuwayama, T., Seinfeld, J. H., and Kleeman, M. J.: Direct measurements of ozone response to emissions perturbations in California, Atmos. Chem. Phys., 22, 4929-4949, 10.5194/acp-22-4929-2022, 2022.

Xiong, Y., Chai, J., Mao, H., Mariscal, N., Yacovitch, T., Lerner, B., Majluf, F., Canagaratna, M., Olaguer, E. P., and Huang, Y.: Examining the Summertime Ozone Formation Regime in Southeast Michigan Using MOOSE Ground-Based HCHO/NO2 Measurements and F0AM Box Model, J. Geophys. Res.-Atmos., 128, 10.1029/2023jd038943, 2023.

https://doi.org/10.5194/egusphere-2026-6618
Preprint. Discussion started: 16 November 2026
© Author(s) 2026. CC BY 4.0 License.

Xu, T., Gao, X., Jiang, S., Hu, K., Peng, Z., Zhao, X., and Tang, X.: Nonlinear ozone response to extreme high temperature in a subtropical megacity basin: Integrated observation and modeling analysis, Environ. Res., 285, 122274, 10.1016/j.envres.2025.122274, 2025.

Yao, T., Lu, S., Wang, Y., Li, X., Ye, H., Duan, Y., Fu, Q., and Li, J.: Revealing the drivers of surface ozone pollution by explainable machine learning and satellite observations in Hangzhou Bay, China, J. Clean Prod., 440, 10.1016/j.jclepro.2024.140938, 2024.

Yildizhan, H., Udriștioiu, M. T., Pekdogan, T., and Ameen, A.: Observational study of ground-level ozone and climatic factors in Craiova, Romania, based on one-year high-resolution data, Sci Rep, 14, 26733, 10.1038/s41598-024-77989-0, 2024.

Zhang, C., Xie, Y., Shao, M., and Wang, Q.: Application of machine learning to analyze ozone sensitivity to influencing factors: A case study in Nanjing, China, Sci. Total Environ., 929, 172544, 10.1016/j.scitotenv.2024.172544, 2024.

Zhang, T.: Interpretative SHAP Value and Partial Dependence Plot, Springer Nature Singapore, 429-462 pp., 10.1007/978-981-99-7992-9_12, 2025.